SCANNING MICROELECTROCHEMICAL TECHNIQUES: A HIGHLY SENSITIVE ROUTE TO EVALUATE DEGRADATION REACTIONS AND PROTECTION METHODS WITH CHEMICAL SELECTIVITY

Ricardo M. Souto[1], Javier Izquierdo[1], Juan J. Santana[2], Sergio González[1]

[1] Department of Physical Chemistry,University of La Laguna, E-38200 La Laguna (Tenerife), Spain

2 Department of Process Engineering, University of Las Palmas de Gran Canaria, Edificio de Ingenierías, E-35017 Gran Canaria, Spain

Abstract

This contribution provides a brief review of the applications of the Scanning Electrochemical Microscope (SECM) and the Scanning Vibrating Electrode Technique (SVET) in measuring, characterising and evaluating surface inhomogeneity and surface chemical activity in the case of heterogeneous materials exposed to aqueous environments. The SECM is a unique microelectrochemical technique that provides *in situ* topographic and electrochemical reactivity information about the surface evolution at the micrometer scale in aqueous solution, thus becoming a very powerful tool in elucidating the complex processes occurring in the early stages of surface films degradation and metal corrosion. On the other hand, the SVET uses a small vibrating probe allowing measurement of the local potential in solution taking advantage of a synchronous detection with a lock-in amplifier. In this way, ionic current related to degradation reactions on an investigated surface can be monitored in the electrolytic phase in contact with the sample. Selected practical examples of some applications of these techniques for the evaluation of degradation reactions and protection methods are presented

Keywords: Scanning microelectrochemistry, degradation, surface layers, chemical activity, organic coatings, oxide films.

1. Introduction

Knowledge about the morphology and chemical activity of heterogeneous materials on micrometer and submicrometer scales is crucial for the comprehensive understanding of the mechanistic aspects of materials degradation initiation and the development of new material properties for highly specified protection. They require the synthesis of data obtained from a number of experimental techniques. Similarly, the stability of surface layers and their resistance against degradation from electrochemical experiments can be

complemented by procedures that reveal the chemical activity and morphology associated with the dynamics and changes occurring during the course of these experiments. In usual electrochemical experiments such as cyclic voltammetry or electrochemical impedance spectroscopy, both heterogeneous rate constant of electron transfer for adsorbed or dissolved species and kinetics of homogeneous coupled chemical reactions can be determined from the analysis of current and potential variations of the electrode [1,2]. Whatever the measurable quantity, it reflects the reactivity of the whole electrode surface; in other words this analysis is based on the assumption that the electrochemical behaviour of the interface is uniform. However, electrodes rarely exhibit such an ideal behavior and the electrode response to a perturbation signal corresponds to an average measurement over the whole electrode surface.

With the development of scanning microelectrochemical techniques it has become possible to gain information about the physical dimensions and morphology of materials, simultaneously providing additional information about their surface chemical activity with a resolution in the micrometer range or below. Such dimensions can be reached by the use of microelectrodes and due to the significant improvement of electronics, devices allowing small current measurements are fabricated. Images with high spatial resolution are thus obtained that provide information on the specific effect of pollutants and the effectiveness of surface layer treatments for materials preservation at microscale. The potential of these techniques for the conservation-restoration of art objects will be illustrated with examples from related fields of applications.

2. Scanning electrochemical microscopy

2.1. Electrochemistry at microelectrodes

Over the last years, the development of high resolution scanning probe microelectrochemical techniques has led to a decrease of the scale of electrochemical processes under investigation down to micrometric and submicrometric ranges. Electrodes of small dimensions, called microelectrodes, are employed, and have provided very useful extension of electrochemical and corrosion fields. The electrochemical behaviour of microelectrodes departs from the conventional electrode, which can be approximated by an electrode of infinite dimension [3]. The differences are caused by changes in the condition of the mass transport from the bulk solution toward the electrode, that occur for a critical dimension in the range 10 nm – 25 μm [3]. This behaviour is included in the definition provided by the IUPAC, which describes the microelectrode as “any electrode whose characteristic dimension is under the given experimental conditions, comparable to or smaller than the diffusion layer thickness” [3].

Though the experiments using microelectrodes are similar to those at "conventional" electrodes, depending on the dimension of the electrode and the volume of the electrolytic solution employed, it is possible to distinguish three limiting cases for diffusion, namely:

- The simplest case is a thin-layer cell with a very low ratio between the cell volume and the electrode surface. In this case, the mass transport within the cell is negligible and no diffusion gradient develops [1].
- By reducing the ratio between the electrode surface and the electrolyte volume, semi-infinite planar diffusion is attained [4,5], as it is shown in the scheme of Figure 1a. This is the situation corresponding to a "conventional electrode".
- When the electrode surface is smaller than the solution volume, the diffusion process becomes dependent on the size and geometry of the electrode [6,7] (see Figure 1b). The diffusive regime is the characteristic feature of microelectrodes in this case.

In the later condition, the diffusion problem is determined by the spherical character of the electrode, and the mass transport process is dominated by radial spherical diffusion. The current attains a time-independent steady state value given by the following expression:

$$i_{SS} = \frac{nFADc_b}{r_o} \qquad (1)$$

where *F*, is the Faraday constant; *r*, the microelectrode radius; *D*, the diffusion coefficient of the reducible species; and, *c*, its concentration. In this case, the steady state response is typical of radial diffusion and arises because the electrolysis rate is equal to the rate at which molecules diffuse to the electrode surface.

Typically, a microelectrode probe is a disk embedded in an infinite insulating plane. The steady-state solution for the microdisk electrode of radius *a* has been obtained [8], and the limiting steady-state current is given by:

$$i_{SS} = 4nFDca \qquad (2)$$

2.2. The technique

The SECM was designed in 1989 by Bard and coworkers [9] by coupling scanning probe techniques with electrochemistry. Since then, the SECM has become a very powerful technique for probing a great variety of electrochemical reactions, due to the combination of its high spatial resolution and its electrochemical sensitivity. The SECM is based in the reaction that

occurs in the surface of a mobile ultramicroelectrode (UME) immersed in an electrolyte solution. The UME is rastered in close proximity to a solid surface to characterize the topography and redox activity of the solid/liquid interface. This latter feature is very important, because it allows SECM to gain information concerning reactions that take place in the solution space between the tip and the sample, as well as on those occurring on the surface of the scanned sample [10]. Thus, the scanning electrochemical microscope can be employed for chemical microscopic imaging, which is especially relevant towards the investigation of corrosion and degradation processes, as well as to measure the efficiency of protection procedures for materials [11,12].

The SECM is a technique in which a current flows through a microelectrode immersed in an electrolytic solution and situated close to a substrate. The substrate can either be a conductive, semiconductive or insulating material. The microelectrode and the substrate form part of an electrochemical cell which also contains reference and auxiliary electrodes, and sometimes by a second working electrode (Figure 2a).

Prior to explaining the operation and the response of the SECM, it is necessary to understand the behaviour of the microelectrode inside an electrochemical cell. Let's consider the microelectrode is immersed in a solution containing an electrolyte and a reducible species, *O*. When a potential sufficiently negative to the standard potential of the reduction reaction (3), is applied to the microelectrode, the reduction of the species *O* occurs at the UME surface, and a cathodic current flows according to:

$$O + ne^- \leftrightarrow R \qquad (3)$$

If this reaction is kinetically controlled by the diffusion of *O* from the bulk of the solution to the electrode surface, the current decays due to the formation of a diffusion layer of *O* around the electrode, and attains rapidly a steady-state value given by equation (2). A steady-state current (see Figure 2b) results from the constant flux of *O* to the electrode surface due to an expanding hemispherical diffusion layer around the microelectrode.

The measurements at an UME, and therefore the measurements at an SECM tip, are no affected by stirring or other convective effects. In SECM, the proximity of the tip to the substrate is the perturbation in the measurement that constitutes the SECM response [9]. If the UME is brought to the vicinity of an insulating substrate, the steady-state current that flows through the tip, i_T, tends to be smaller than $i_{T,\infty}$ (Figure 3a).

This is a result of the insulating substrate partially blocking the diffusion of *O* towards the tip [13]. The current at the tip becomes smaller when the tip is closer to the substrate, and tends to zero when the distance between tip and substrate, *d*, approaches zero. This effect is known as negative feedback.

In contrast, if the tip is close to a conductive substrate at which the oxidation reaction (4) can occur, a flux of *O* from the substrate to the tip occurs, in addition to some flux from the bulk solution towards the tip.

$$R \leftrightarrow O + ne^- \quad (4)$$

This effect leads to an enhancement of the current at the tip, i_T, which is higher than $i_{T,\infty}$ (Figure 3b). Then the flux of *O* from the substrate to the tip causes an increase of i_T as *d* decreases. In this case, when the tip-substrate distance approaches zero, the i_T current tends to infinite, and the oxidation of *R* on the substrate is diffusion-controlled. This effect is named positive feedback. The tip can be seen as both the generator of the signal sensing the substrate (the flux of the reduced species, *R*), and the detector (of the flux of *O* from the substrate).

2.3. The SECM setup

The SECM instrument consists of a combination of electrochemical components and some components of the scanning probe microscopies (SPM). A diagram with the main components of the scanning electrochemical microscope is shown in Figure 4.

It consists of four major parts: (1) The electrochemical cell, which is formed by the tip, the counterelectrode, the reference electrode and the substrate that occasionally, can act as second working electrode; (2) the bipotentiostat, which constitutes the SECM electrochemical setup together with the electrochemical cell; (3) the tip movement and position controller, which is the SPM component; and (4) the computer, interface and display system.

The SECM instrument used in the experiments was a Sensolytics scanning electrochemical microscope (Sensolytics, Bochum, Germany), with a bipotentiostat (Palmsens, Utrecht, The Netherlands) as the electrochemical interface. Control motion of the microelectrode was performed using a step motor driven *x*-, *y*-, *z*-stage (Owis GmbH, Staufen, Germany) capable of reproducible three-dimensional motion. A disk-shaped Pt microelectrode (10 μm diameter) was employed as working electrode, an iridium wire as counter, and an Ag/AgCl/KCl (3M) as reference electrode.

2.4. Practical examples of SECM measurements

In the following, practical examples of some applications of this technique will be presented.

2.4.1 Surface imaging of polymer coated metals

The SECM can be employed to image the surfaces of different types of substrates, both insulators and conductors, immersed in solutions. In this case, the SECM operates in the *feedback* mode. Then, it is necessary an oxidizable/reducible species in the solution which is known as redox mediator (cf. Figure 3). Generally redox couples involving a fast, usually one-electron, heterogeneous reaction at the tip are chosen as electrochemical mediators. In this mode, the SECM tip is rastered in the *X*-*Y* plane of the surface of the sample inside an electrochemical cell. The faradaic current measured at the tip is controlled by diffusion of the mediator, and depends strongly on the tip-sample separation. The variations in the measured current are related to changes in the tip-sample distance and therefore, they are related to the topography of the sample.

Surface images are often determined with the SECM operating in the *constant height* mode. In this way, the tip is lowered to a fixed distance from the substrate and then the surface is scanned. In this case, the currents measured at the tip can be rapidly converted to a height or distance scale. The resolution of the SECM in topographic measurements on a surface strongly depends on the tip radius, *a*.

Coating a metallic substrate with a polymeric coating constitutes an efficient protection procedure against corrosion as it introduces a physical barrier layer that separates the metal from the environment. But this organic layer cannot provide an absolute separation between the underlying substrate and the electrolyte because permeation of water and oxygen through the polymer matrix occurs even for defect-free coated metals immediately after exposure to aqueous electrolytes. Using SECM, it has been demonstrated that pollutants such as chloride ions produces swelling of the coating and even early blister initiation at very early exposures in a variety of metal-polymer systems could be observed by SECM operating in the feedback mode [14-16]. This method requires the measurement of a faradaic current at the SECM tip, and topographic changes in an insulating surface such as the defect-free coated metal originate from local hindrance in the diffusion-limited transport of the redox mediator as the tip is moved in close proximity to the surface. In this way, the uptake of chemical species from the electrolyte phase through the polymeric matrix to the metal/polymer interface can be investigated even at early exposures.

Figure 5 shows topographic images of carbon steel samples coated with an epoxy primer for corrosion protection. The coated samples were left unbiased during the experiments at their corresponding open-circuit potential. The images were measured by SECM operated in the negative feedback mode, using 0.5 mM ferrocene-methanol added to the corresponding electrolyte. The test environments considered were doubly-distilled water (A), 0.05 M NaCl (B), and 0.5 M NaCl (C). They were chosen as to separate the uptake of water by the

polymeric layer from eventual transport processes due to ions in the aqueous phase, and whether the later may occur above a minimum concentration of the chemical species, respectively. SECM images taken after 24 hours exposure to the test solutions show featureless surfaces in the case of pure water and for the dilute NaCl solution (c.f.. the maps labelled A and B), a clear indication that transport processes in the system are of a homogeneous nature and involve only water. Conversely, heterogeneous swelling of the coating surface occurred in the more concentrated NaCl solution, with the observation of bulges in the material (see Figure 5C). They are regarded to be localized sites for the accumulation of a concentrated saline solution at the metal-polymer interface, which may act as locations where the corrosive attack of the underlying metal is initiated. In this way, a specific effect of chloride ions towards heterogeneous distribution of chemical species in a coated metal is described, which requires a critical concentration of the aggressive species to occur. In this case, the effect took place when the concentration of chloride ions in the environment was 0.5 M but it was not found for the lower concentration tested.

This method can be applied as described when no measurable lixiviation of chemical species from the polymer matrix occurs. But in the event there are transport processes from the organic matrix into the solution phase, such as those related to lixiviation, the topography of the polymer layer may evolve with time accordingly, not longer exclusively responding to the uptake by the polymer matrix of components from the electrolyte phase. Bidirectional transport then occurs in the system, and experimental procedures must be developed to separate both contributions to the total SECM response [17].

2.4.2 Detection of localized pitting corrosion initiation on stainless steel

The SECM can be employed to image the chemical activity of materials with spatial resolution, as to discover whether the initiation of corrosion occurs locally (i.e. localized corrosion) or it is distributed rather homogeneously over the whole exposed surface of the material (homogeneous corrosion). Figure 6 shows experimental results for SECM measurements performed on 304 stainless steel in a 0.25 M HCl solution at the equilibrium potential (E_{oc}) and polarized positively with respect to E_{oc}. The microelectrode tip consisted of a platinum wire of diameter 25 μm insulated laterally by glass, leaving a disk as the electrochemically-active surface. The tip was positioned at XX μm above the steel sample with ca. 1x1 mm^2 to form the testing metal substrate. This metal coupon was embedded into an epoxy resin sleeve, such that only the square end surface forms the testing surface.

Stainless steel spontaneously passivates in this aggressive environment, producing a stationary passive current. That is, metal dissolution is prevented by the development of an oxide layer enriched in chromium at the surface of the metal, though at the cost of some preferential dissolution of iron. Iron dissolves as Fe(II) ions which diffuse from the surface towards the bulk of the electrolytic

environment. The release of these soluble iron species offers an alternate operation scheme for SECM thus making unnecessary the addition of an external redox mediator for imaging purposes. In this case, the species generated at the passivating surface can be collected at the tip to be further oxidized to oxidation state +3 at the tip according to:

$$Fe^{2+} \leftrightarrow Fe^{3+} + e^{-} \quad (4)$$

The faradaic current associated to this oxidation will be directly proportional to the concentration of the species at the location scanned by the tip. This operation proceduree is called the generation-collection mode of SECM. Oxidation of Fe(II) soluble species at the tip was secured by setting the tip potential at +0.50 V vs. Ag/AgCl/KCl (3M) reference electrode.

Figure 6A shows the SECM image obtained when the steel sample was left at the equilibrium potential (E_{oc} = -0.25 V vs. Ag/AgCl/KCl (3M)). The onset of passivity is observed as an increase of the faradaic current measured at the tip when passing above the metal sample, whereas significantly smaller (residual) currents were observed over the surrounding resin, which corresponded to the soluble species diffusing away from the metal sample into the bulk of the solution. Constant faradaic currents averaging 0.48 nA are measured over the entire surface of the metal exposed to the environment.

Conversely, a heterogeneous current distribution over the steel sample was observed after polarizing the sample at potential values positive with respect to E_{oc}, and indication of localized electrochemical activation of the metal surface.

Anodic polarization of the sample effectively removes electrons from the steel. Activation of two separated spots on the surface of the metal is observed in the SECM map depicted in Figure 6B, which are viewed as regions of significantly higher faradaic currents for the oxidation of Fe^{2+} ions than the rest of the material. The currents measured at the tip above those two electrochemically hot spots are ca. 8 times bigger than the background passive current measured for the unbiased sample (cf. Figure 6A). They are regarded to be nucleation spots for metastable pits [18]. Further polarization of the sample to +0.05 V vs. Ag/AgCl/KCl (3M) leads to the observation of a propagating pit at the top of the image shown in Figure 6C. That is, the rate of corrosion in that pit has greatly increased, leading to a much bigger hole than observed at the less anodic potential. Conversely, the other pit observed in the lower half of Figure 6B, continues corroding without a significant increase of either the size or the dissolution rate associated with it. SECM maps greatly assist to unveil localized forms of corrosion which are very hazardous for the integrity of the material such as pitting corrosion. In this case, metal dissolution occurs at a very high rate in rather small areas of the exposed surface, thus mostly leading to perforation of the material, whereas the surrounding metal exposed to the

environment remains passive and actually behave as the cathode of the corroding electrochemical cell.

3. Scanning vibrating electrode technique

Whereas the SECM method is based on the measurement of a Faradaic (redox) current at the sensing tip, the scanning vibrating electrode technique is based upon the measurement of potential field distributions in the electrolyte surrounding an electrochemically active surface.

3.1. The technique

The Scanning Vibrating Electrode Technique (SVET) is known since 1950, a method originally devised by biologists for the measurement of extracellular currents around living cells [19-22]. But it was only in the seventies that it was applied to the investigation of corrosion processes for the first time [23,24].

The SVET is a technique that allows the detection of ionic currents in a solution caused by a concentration gradient. It is based in the detection of electric fields generated in a solution due to homogeneous distribution of electric charges such as ions. The electric field is zero when the solution is at rest, but if there is a gradient of concentration caused by a source of ions, a variation of potential in the solution occurs (see Figure 7). Ionic flows can arise from corrosion processes on a metal. The oxidation reactions occurring at anodic sites on a metal surface in contact with an electrolyte cause electrons to flow through the metal substrate to adjacent cathodic areas. This flow of electrons through the metal is supported by a flow of ionic current in the electrolyte, which in turn causes potential gradients to exist in the solution close to sites of localised corrosion.

However, these gradients in the solution are so small that they cannot be detected using conventional techniques. The scanning vibrating electrode technique uses a microelectrode fixed in the solution and another vibrating microelectrode that scans the surface to measure these gradients *in situ*. Measurement is made by vibrating a fine tip microelectrode a few hundred microns above the sample, usually in a plane perpendicular to the surface (cf. Figure 8).

The electrochemical potential of the microelectrode is recorded at the extremes of the vibration amplitude, resulting in the generation of a sinusoidal *AC* signal, given by:

$$h(t) = h_0 + d\text{sen}(\Omega t) \quad (5)$$

where d is the amplitude of the microelectrode vibration, Ω is the angular frequency of the vibration, and h_0 is the average distance between the electrode and the sample. Then this signal is measured using a *lock-in* amplifier, which is tuned to the frequency of probe vibration. The measured potential variation, ΔV, can be related with the ionic currents by use of the equation:

$$I = \frac{E}{\rho} = \frac{1}{\rho}\frac{\Delta V}{\Delta r} \quad (6)$$

where E is the electric field measured between two points of the solution, ρ is the resistivity of the solution, and Δr the distance between the two extremes or vibration amplitude of the microelectrode.

3.2. The SVET setup

A scheme of the main components of the technique is shown in Figure 9-left. Thus, the scanning vibrating electrode instrument is basically constituted by: (1) the electrochemical cell; (2) the piezo-oscillator system which produces the vibration of the microelectrode; (3) two *lock-in* amplifiers that measure and filter the signal produced in the probe; (4) tri-axial piezoelectric motors to control with precision the movement and the position of the vibrating probe; and (5) the computer, interface and display system.

The electrochemical cell consists of the vibrating and fixed microelectrodes, the reference electrode, and the sample. Figure 9-right shows the distribution of the elements in the cell.

3.3. Practical examples of SVET measurements

In the following, practical examples of some applications of this technique will be presented.

3.3.1 Detection of localized chemical heterogeneities at aluminium alloys

For the SVET measurements, bare aluminium alloy was introduced in the teflon cell and exposed to 50 mM NaCl as test environment. This technique is more sensitive at relatively low ionic strength solutions, as it is able to detect

differences in potential due to the presence of extra amounts of ionic charges in the vicinity of the surface, and the lower the concentration, the higher the relative proportion of the extra ions is. On the other side, one needs to establish a compromise situation as sufficiently aggressive media is required to promote corrosion and thus to monitor results.

In situ SVET acquisitions in the electrolyte are displayed in Figure 10. Maximum and minimum current density values are comparable to those encountered in the literature for the same media though measured at bigger distances from the substrate [25,26]. The closer height selected in this work, in combination with the reduction of the amplitude vibration, allows us to better distinguish the reacting sites. It can be noticed that, while most of the metal surface is behaving slightly cathodic, some areas are activated anodically during the exposure to chloride anions, and they remain under attack for several hours.

Inded, the location of coordinates (X = 1120 μm, Y = 900 μm) appears anodically-activated in Figure 10B, recorded after 5 hours immersion of the sample in the electrolyte, and remains active in Figure 10C taken 4 hours later. The photographs taken just before each scan, show the accumulation of corrosion products at that position.

The dimensions of the developed pits are in the order of 100 μm diameter, which is consistent with the SVET results found in the previous papers cited before. However, we would expect to detect the effect of the Al(CuMnFe) particles, which behave cathodic with respect to the matrix, yet what can be visualized consists on local anodic sites, that cover greater areas than those expected for any of the possible intermetallics. This feature can be temptatively explained in terms of two different options:

- Anodic dissolution occurs in the matrix via pitting corrosion, promoted by the galvanic connection with the noblest particles. The cathodic half-reaction on them is not easily detected since their size is too small to be spatially resolved by SVET. In that case, the dissolution of anodic intermetallics and its eventual removal from the surface may be acting as the initial stage of pit formation, leading to the exposure of a weaker area to the electrolyte.
- Cu-rich particles, either Al(CuMnFe) intermetallics or the s-phase of the base metal once lost its Mg content, mainly promote the dissolution of the surrounding material, resulting in the degradation of the matrix around them reaching active diameters up to 5 times greater than that of the original particle [27-34]. Conversely, SVET would detect the anodic current on their proximity, but probably it will not be able to resolve the anionic current emerging locally from the inclusion in the centre of the active location.

Our SVET results may well adjust to both explanations. Observations encountered using AC-SECM showed some degradation in the proximity of some active sites and subsequent topographic changes during deactivation of the surface [35], what would be better explained by the second possibility. However, the media employed for the SVET measurements is more aggressive

that the one employed in the reported work, so the results described here may correspond to a later stage in the degradation of the material which corresponds to pit formation in the alloy. In fact, according to the literature, the whole corrosion process of this material will followed by pit formation and intergranular corrosion [25,36,37].

3.3.2 Detection of localized chemical heterogeneities at aluminium alloys

Aluminium alloys can be effectively protected from corrosion by coating the material with a zirconia layer [38]. Indeed, no electrochemical activity was detected by SVET when the coated samples were immersed in 50 mM NaCl aqueous solution. A new series of experiments was performed on a sample that was scratched until the underlying AA2024 alloy was exposed to the environment inside the defect (cf. Figure 11A). At the beginning of the experiment, only a very small electrochemical activity could be detected inside the scratch when recording the SVET image with high sensitivity.

With the elapse of time, onset of corrosion inside the defect is observed through the progressive development of two greatly localized anodic sites, whereas the remaining uncoated metal serves as the cathode for the consumption of the electrons liberated by the corroding metal. SVET has allowed the detection of distributed corrosion microcells inside the defect through the zirconia coating with great spatial resolution. That is, once the zirconia coating is perforated as to not longer effectively separate the underlying aluminium alloy from the environment, the corrosion mechanism operating in the uncoated material is also operating inside the defect. Therefore, an effective protection method for aluminium based on the use of zirconia as physical barrier film must also include self-healing mechanisms capable of repairing the perforated film, possibly through the controlled release of corrosion inhibitor compounds.

5. Conclusions

Scanning microelectrochemical techniques offer a powerful route to investigate the onset of corrosion reactions in a wide variety of technologically interesting materials, as well as to effectively characterize the protection efficiency of different protection methods. The main advantage of these methods is their ability to detect and quantify the electrochemical activity of materials related to the onset of degradation reactions with spatial resolution.

Acknowledgement

The authors are the beneficiaries of the projects CTQ2009-12459 and CTQ2009-14322 co-funded by the European Regional Development Fund

(Brussels, Belgium) and by the Ministerio de Ciencia e Innovación (Madrid, Spain). A Research Training Grant awarded to J.I. by the Ministerio de Educación (Programa de Formación de Personal Investigador, Madrid, Spain) is gratefully acknowledged.

References

[1] A.J. Bard and L.R. Faulkner, *Electrochemical Methods: Fundamentals and Applications*, 2nd edn., Wiley-VCH, New-York, 2001.
[2] C. Gabrielli, in *Physical Electrochemistry. Principles, Methods, and Applications*, I.Rubinstein (ed.), Marcel Dekker, New-York, 1995, Ch. 6.
[3] K. Štulík, C. Amatore, K. Holub, V. Mareček and W. Kutner, Pure and Applied Chemistry, **72** (2000) 1483.
[4] J. Heinze, Angewandte Chemie, **96** (1984) 823.
[5] J. Heinze, Angewandte Chemie International Edition, **168** (1984) 831.
[6] R.M. Wightman and D.O. Wipf, in *Electroanalytical Chemistry*, vol. 15, A.J. Bard (ed), Marcel Dekker, New York, 1989.
[7] A.M. Bond, K.B. Oldham and C.G. Zoski, Analytica Chimica Acta, **216** (1989) 177.
[8] Y. Saito, Review of Polarography (Japan), **15** (1968) 177.
[9] A.J. Bard, F-R.F. Fan, J. Kwak and O. Lev, Analytical Chemistry, **61** (1989) 132.
[10] A.L. Barker, M. Gonsalves, J.V. Macpherson, C.J. Slevin and P.R.Unwin, Analytical Chimica Acta, **385** (1999) 223.
[11] J.V. Macpherson and P.R. Unwin, in *Scanning Electrochemical Microscopy*, A.J. Bard and M.V. Mirkin (eds.), Marcel-Dekker, New York, 2001, 521.
[12] L. Niu, Y. Yin, W. Guo, M. Lu, R. Qin and S. Chen, Journal of Materials Science, **44** (2009) 4511.
[13] A.J. Bard, G. Denuault, C. Lee, D. Mandler and D.O. Wipf, Accounts of Chemical Research, **23** (1990) 357.
[14] R.M. Souto, Y. González-García, S. González and G.T. Burstein, Corrosion Science, **46** (2004) 2621.
[15] R.M. Souto, Y. González-García, S. González and G.T. Burstein, Electroanalysis, **21** (2009) 2569.
[16] Y. González-García, J.J. Santana, J. González-Guzmán, J. Izquierdo, S. González and R.M. Souto, Progress in Organic Coatings, **69** (2010) 110.
[17] R.G. Duarte, S. González, A.S. Castela, M.G.S. Ferreira and R.M. Souto, Progress in Organic Coatings, **74** (2012) 365.
[18] Y. González-García, G.T. Burstein, S. González and R.M. Souto, Electrochemistry Communications, **6** (2004) 637.
[19] O. Bluh and B. Scott, Review of Scientific Instruments, **10** (1950) 867.
[20] L.F. Jaffe and R. Nucitelli, Journal of Cell Biology, **63** (1974) 269.
[21] D. Mackenzie, New Scientist, **28** (1982) 217.
[22] A.M. Shipley and J.A. Feijó, in *Fertilization in Higher Plants. Molecular and Citological Aspects.* Springer-Verlag, Berlin, 1999, Ch. 17.
[23] H.S. Isaacs, Corrosion, **43** (1987) 594.
[24] H.S. Isaacs, Corrosion Science, **28** (1988) 547.
[25] K.A. Yasakau, M.L. Zheludkevich, O.V. Karavai and M.G.S. Ferreira, Progress in Organic Coatings, **63** (2008) 352.

[26] S.M. Tamborim, S.L.P. Dias, S.N. Silva, L.F.P. Dick and D.S. Azambuja, Corrosion Science, **53** (2011) 1571.
[27] R.G. Buchheit, R.P. Grant, P.F. Hiava, B. Mckenzie and G.I. Zende, Journal of the Electrochemical Society, **144** (1997) 2621.
[28] R.P. Wei, C.-M. Liao and M. Gao, Metallurgical and Materials Transactions A, **29** (1998) 1153.
[29] P. Campestrini, H.W. van Rooijen, E.P.M. van Westing and J.H.W. de Wit, Materials and Corrosion, **51** (2000) 616.
[30] T. Suter and R.C. Alkire, Journal of the Electrochemical Society, **148** (2001) B36.
[31] K.A. Yasakau, M.L. Zheludkevich, S.V. Lamaka and M.G.S. Ferreira, Journal of Physical Chemistry B, **110** (2006) 5515.
[32] F.M. Queiroz, M. Magnani, I. Costa and H.G. de Melo, Corrosion Science, **50** (2008) 2646.
[33] A. Boag, A.E. Hughes, A.M. Glenn, T.H. Muster and D. McCulloch, Corrosion Science, **53** (2011) 17.
[34] A.E. Hughes, A. Boag, A.M. Glenn, D. McCulloch, T.H. Muster, C. Ryan, C. Luo, X. Zhou and G.E. Thompson, Corrosion Science, **53** (2011) 27.
[35] J. Izquierdo, B. Socas, S. González and R.M. Souto, submitted.
[36] C.H. Paik, H.S. White and R.C. Alkire, Journal of the Electrochemical Society, **147** (2000) 4120.
[37] F. Andreatta, H. Terryn and J.H.W. de Wit, Electrochimica Acta, 49 (2004) 2851.
[38] F. Andreatta, L. Paussa, P. Aldighieri, A. Lanzutti, D. Ondratschek and L. Fedrizzi, Surface and Interface Analysis, **42** (2010) 293.

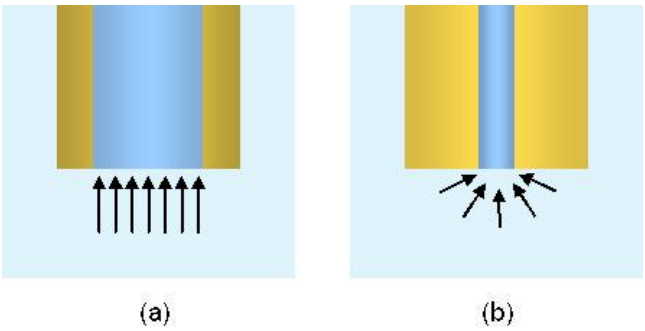

Figure 1. Scheme of the geometry and diffusion field for (a) conventional electrode, and (b) microelectrode.

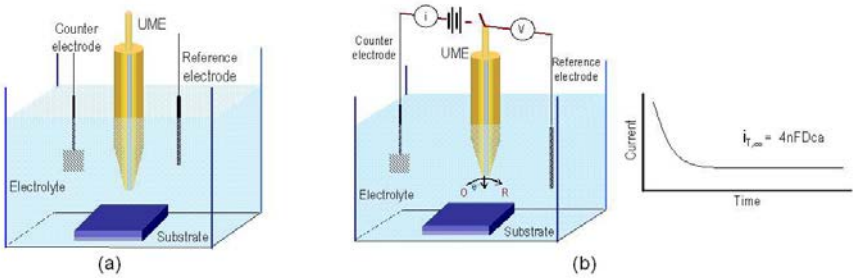

Figure 2. Sketch of an electrochemical scanning microscope. (a) The UME is immersed in a solution containing a redox species *O*. (b) The potential at the UME is set to a value at which the species O can be reduced to *R* under diffusion limiting conditions. The current trace recorded at the UME in the later condition is also given.

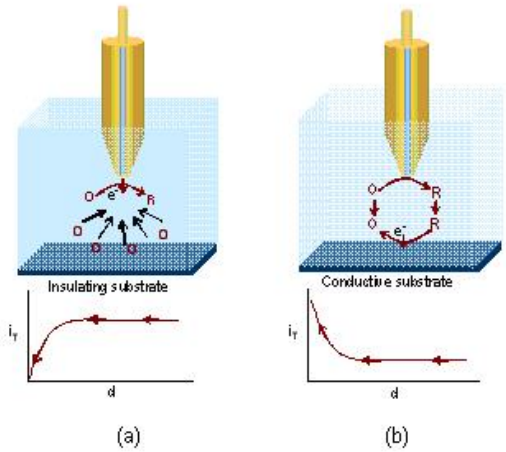

Figure 3. Basic principle of SECM: (a) Negative feedback: the tip is placed near an insulating substrate which hinders the diffusion of species *O*. (b) Positive feedback: the tip is located near a conductive substrate where the oxidation of species *R* occurs.

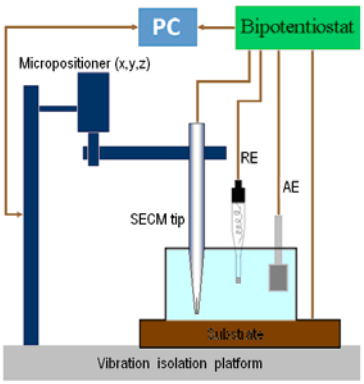

Figure 4. Scheme of the basic components of a SECM equipment, including the SECM tip, reference electrode (RE) and auxiliary electrode (AE).

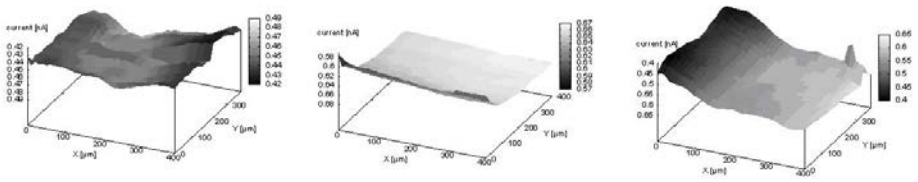

Figure 5. SECM images of steel substrates painted by an epoxy coating after 24 hours immersion in: (A) pure water, (B) 0.05 M NaCl, and (C) 0.5 M NaCl solutions. 0.5 mM ferrocene-methanol was added to the test solutions as redox mediator. Values of *Z* axis: Current, nA. Redox mediator: oxygen. Tip potential: +0.50 V vs. Ag/AgCl/KCl (saturated) reference electrode. Tip diameter: 10 μm. Tip-substrate distance: 15 μm. The images represent 800 μm x 800 μm in *X* and *Y* directions.

Figure 6. SECM images of a 304 steel sample immersed in 0.25 M HCl solution. Polarization of the sample: (A) unbiased (E_{oc} = -0.25 V vs. Ag/AgCl/KCl (3M)), (B-C) polarized at (B) -0.10, and (C) +0.05 V vs. Ag/AgCl/KCl (3M)). Values of *Z* axis: Current, nA. Redox mediator: dissolved Fe^{2+} ions. Tip potential: +0.50 V vs. Ag/AgCl/KCl (3M) reference electrode. Tip diameter: 25 μm. Tip-substrate distance: 15 μm. The images represent 2000 μm x 2480 μm in *X* and *Y* directions.

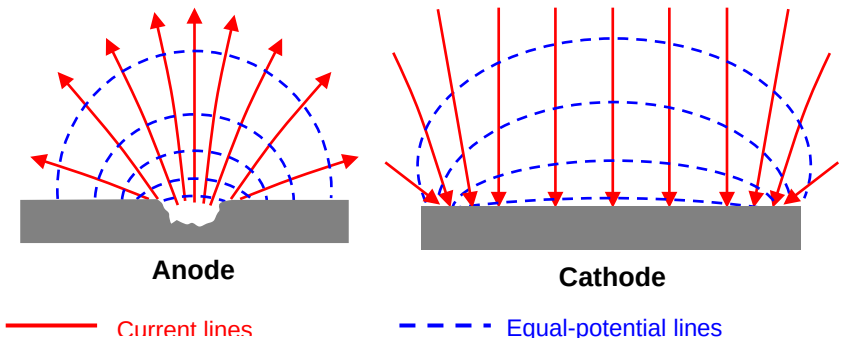

Figure 7. Scheme of current lines and equal-potential lines, which arise from (a) an anodic point while (b) the rest of the surface acts as a cathode.

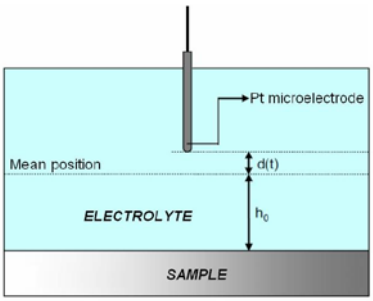

Figure 8. Sketch of the scanning vibrating electrode technique. The Pt microelectrode is vibrated perpendicular to the surface of the investigated substrate while immersed in a solution of low conductivity.

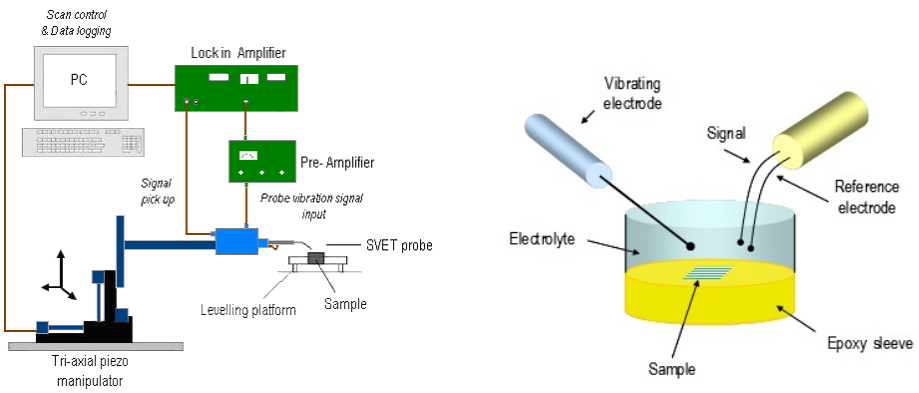

Figure 9. (left) Scheme of the basic components of a SVET equipment, including the SVET probe. (right) Components of the electrochemical cell of the SVET and its general function.

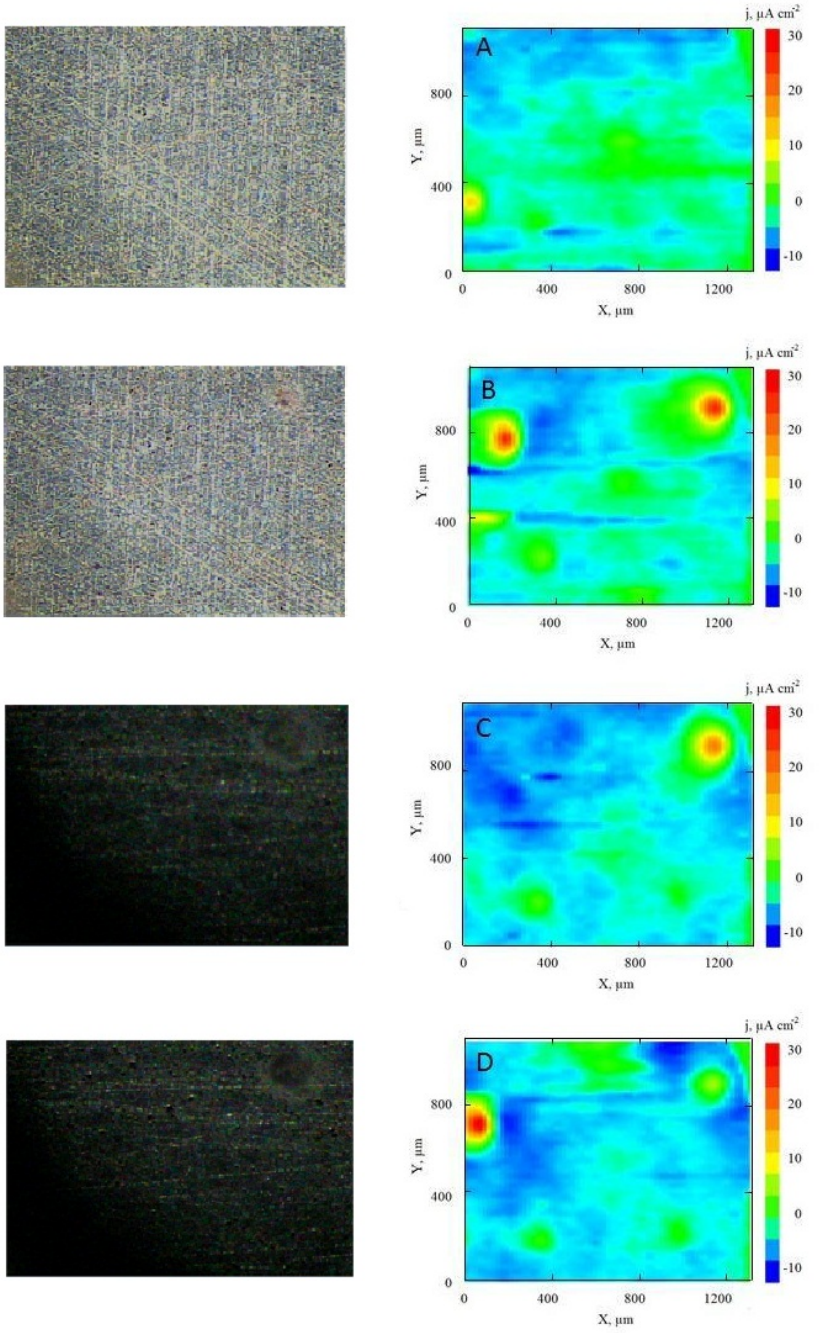

Figure 10. SVET images and micrographs of AA2024 alloy immersed in 50 mM NaCl aqueous solution for: (A) 4, (B) 5, (C) 9, and (D) 11 hours. Values of *Z* axis: Ionic current, µA cm^{-2}. Tip-substrate distance: 15 µm. The images represent 1000 µm x 1300 µm in *X* and *Y* directions.

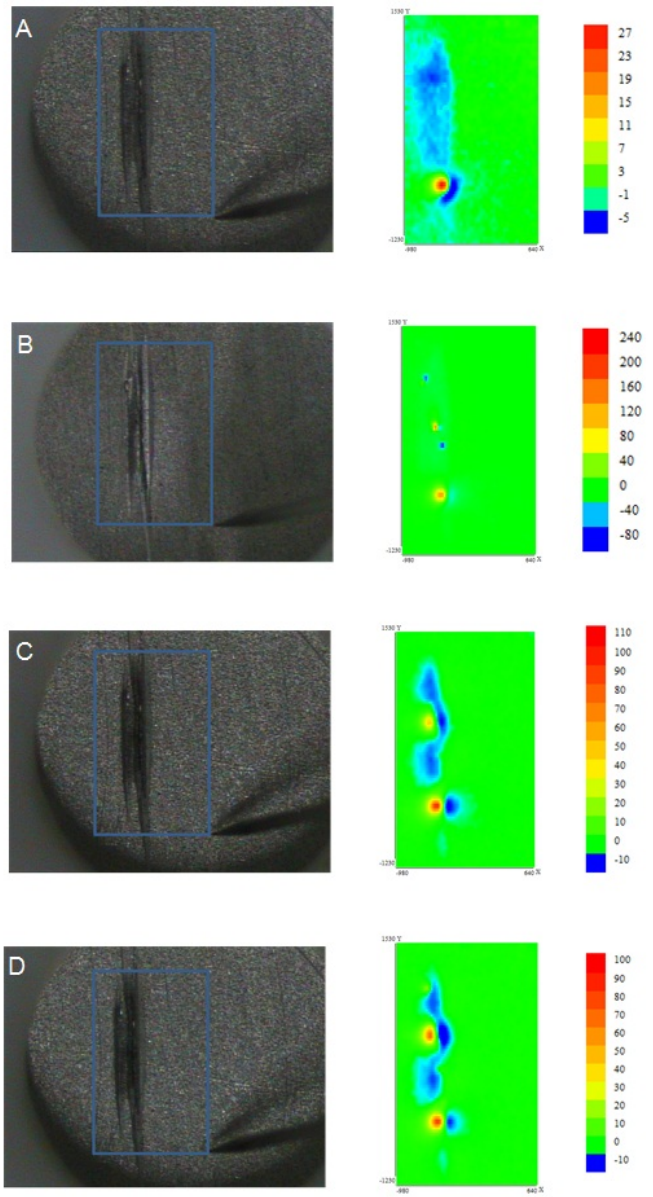

Figure 11. SVET images and micrographs of AA2024 alloy coated by zirconia. A scratch was performed through the zirconica layer to expose the underlying metal to the test environment, 50 mM NaCl Time immersion in NaCl 50 mM: (A) 1, (B) 60, (C) 200, and (D) 320 min. The blue rectangle on the micrographs indicates the scanned area covered by the SVET images. Values of *Z* axis: Ionic current, μA cm^{-2}. Tip-substrate distance: 50 μm. The images represent 1000 μm x 1300 μm in *X* and *Y* directions.